7-15-2017

Trilobite Extinctions, Facies Changes and the ROECE Carbon Isotope Excursion at the Cambrian Series 2–3 Boundary, Great Basin, Western USA

Luke E. Faggetter
University of Leeds

Paul B. Wignall
University of Leeds

Sara B. Pruss
Smith College, spruss@smith.edu

Robert J. Newton
University of Leeds

Yadong Sun
Friedrich-Alexander-Universität Erlangen-Nürnberg

See next page for additional authors

Trilobite extinctions, facies changes and the ROECE carbon isotope excursion at the Cambrian Series 2 - 3 boundary, Great Basin, western USA.

Faggetter, Luke E.[a]; Wignall, Paul B.[a]; Pruss, Sara B.[b]; Newton, Robert J.[a]; Sun, Yadong [c]; Crowley, Stephen [d];

[a] The School of Earth and Environment, the University of Leeds, Leeds, West Yorkshire, LS2 9JT, United Kingdom. ee08lef@leeds.ac.uk; P.B.Wignall@leeds.ac.uk; r.j.newton@leeds.ac.uk; [b] Department of Geosciences, Smith College, Northampton, MA 01063, United States. spruss@smith.edu; [c] School of Geography and Earth Sciences, Friedrich-Alexander University Erlangen-Nürnberg, Schloßgarten 5, 91054 Erlangen, Germany. yadong.sun@cug.edu.cn; [d] School of Environmental Sciences, University of Liverpool, Jane Herdman Building, Liverpool L69 3GP, United Kingdom. sfcrow@liverpool.ac.uk.

Corresponding author: Luke Faggetter, ee08lef@leeds.ac.uk.

Abstract

The mass extinction of the olenellid trilobites occurred around the Cambrian Series 2 - Series 3 boundary. Like many other crises, it coincided with a negative carbon isotope excursion but the associated palaeoenvironmental changes remain unclear. To investigate the causal mechanism for this event, we report facies changes, pyrite framboid petrography and carbon isotope values from Cambrian Series 2 - Series 3 (traditionally Early - Middle Cambrian) boundary strata of the Carrara Formation (Death Valley region, California) and Pioche Formation (Nevada). These data reveal regionally changing water depths from high-energy, nearshore facies (oolitic grainstone) to more offshore silty marl and finer-grained carbonate mudstone. In the Carrara Formation, the series boundary occurs within a deepening succession, transitioning from high-energy, nearshore facies (oolitic grainstone and oncolitic packstone) to offshore marl, the latter of which contains pyrite framboid populations indicative of low-oxygen (dysoxic) depositional conditions. Intermittent dysoxia persisted below sub-wave base settings throughout the early and middle Cambrian, but did not intensify at the time of extinction, arguing against anoxia as a primary cause in the olenellid trilobite extinction. Within both field areas, the extinction interval coincided with a minimum in $\delta^{13}C_{carb}$ values, which we interpret as the regional manifestation of the Redlichiid-Olenellid Extinction Carbon isotope Excursion (ROECE). The Series 2 - Series 3 boundary is reported to closely coincide with a large-amplitude sea-level fall that produced the Sauk I/II sequence boundary, but the placement of the Series 2 - Series 3 boundary within a transgressive interval of the Carrara Formation shows that this is not the case. The main sequence boundary in the succession occurs much lower in the succession (at the top of the Zabriskie Quartzite) and therefore precedes the extinction of the olenellids and ROECE.

Keywords: Olenellid extinction, Carrara Formation, Pyramid Shale Member, Pioche Formation, C-Shale Member

1. Introduction

The first major biotic crisis of the Phanerozoic occurred during the Cambrian Series 2, an interval that saw the collapse of archaeocyathan reefs (Newell, 1972; Boucot, 1990; Debrenne, 1991; Zhuravlev and Wood, 1996). This was followed, at the Series 2 - Series 3 boundary, by severe generic-level losses of olenellid and redlichiid trilobites (Palmer, 1998; Zhu et al., 2004; Zhu et al., 2006; Fan et al., 2011; Wang et al., 2011; Zhang et al., 2013). This trilobite extinction has been used to delineate the Series 2 - Series 3 boundary; however, the boundary remains unratified as international correlation is confounded by a lack of globally-distributed taxa at this time (Sundberg et al., 2016). The trilobite extinction coincides with a major negative $\delta^{13}C$ excursion that has been termed the Redlichiid-Olenellid Extinction Carbon Isotope Excursion or ROECE (Zhu et al. 2004, 2006).

In the western Great Basin of the United States, a Cambrian sedimentary succession developed on a rapidly subsiding passive margin (Prave, 1999; Stewart, 1972; Fedo and Cooper, 2001; Hogan et al., 2011; Keller et al., 2012; Morgan, 2012). Sections in the southern Nopah Ranges (Keller et al., 2012) expose strata from Cambrian Sauk I and Sauk II supersequences that are of importance to this study (Prave, 1991). These are widespread, large-scale Laurentian sequences that provide a regional stratigraphic framework. The transition from Sauk I to Sauk II records a major lithological change that saw the siliciclastic deposition of the Zabriskie Quartzite replaced by carbonate deposition of the Carrara Formation (Keller et al., 2012; Morgan, 2012). The contact between these two units is considered to be the Sauk I/II sequence boundary (Keller et al., 2012; Morgan, 2012).

Throughout the Phanerozoic the relationship between environmental perturbation and extinction is a common focus of studies, including those in the Cambrian (Hallam and Wignall, 1997; Wignall, 2015). In particular, sea-level change, marine anoxia, carbon isotope excursions and eruptions of LIPs (large igneous provinces) often coincide with mass extinctions (Zhuravlev and Wood, 1996; Wignall, 2001; Glass and Phillips, 2006; Jourdan et al., 2014). Thus, Zhuravlev and Wood (1996) noted the temporal link between widespread deposition of black shales and the disappearance of the archaeocyathans in the Cambrian of Siberia, and trilobite extinctions at "biomere" boundaries are also ascribed to dysoxia (Palmer, 1984). However, the role of anoxia in Cambrian extinctions has to be viewed in the context of persistently oxygen-restricted oceans at this time (e.g. Montañez et al., 2000; Hurtgen et al., 2009; Pruss et al., 2010; Gill et al., 2011; Saltzman et al., 2015; Tarhan et al., 2015).

Volcanism may also have played a role in ROECE (Glass and Phillips, 2006). The Kalkarindji LIP is a Cambrian flood basalt province of northern and central Australia with an estimated original surface area of ~ 2.1×10^6 km^2 (Glass and Phillips, 2006; Jourdan et al., 2014; Marshall et al., 2016).

Latest dating efforts yield a zircon age of 510.7 ± 0.6 Ma, which is close to that of the Cambrian Series 2 - Series 3 boundary (Jourdan et al., 2014).

In order to improve our understanding of the events associated with ROECE, this study examines sections spanning the Cambrian Series 2 - Series 3 boundary interval in the western Great Basin. The olenellid extinction horizon has been located within the Pioche Formation in Nevada (Palmer, 1998). We have examined this level and the correlative levels in the Carrara Formation in California in order the examine changes of lithofacies, carbon isotope variability and pyrite petrography.

2. Geological background and biostratigraphy

Following breakup of the Rodinia supercontinent in the late Neoproterozoic, the northwestern margin of Laurentia subsided rapidly (Bond and Kominz, 1984; Levy and Christie-Blick, 1991; Prave, 1999; Howley et al., 2006). By the early Cambrian, the western Great Basin (USA) was positioned along the western margin of Laurentia where a wide, clastic-dominated shelf developed in an equatorial setting (Palmer and Halley, 1979; MacNiocaill and Smethurst, 1994; Fig. 1). Clastic input decreased in late Series 2 and was replaced by carbonate deposition (Erdtmann and Miller, 1981; Howley et al., 2006; Landing, 2012).

We have assessed environmental conditions across the Series 2 - Series 3 boundary from sections in the Great Basin including Emigrant Pass (Nopah Range, Death Valley, eastern California), and Oak Springs Summit (Burnt Springs Range, eastern Nevada; Fig. 1). The regional lithostratigraphy of the Pioche Formation (at Oak Springs Summit) was described in detail by Merriam and Palmer (1964), and the Carrara Formation (at Emigrant Pass) by Palmer and Halley (1979). In addition, we examined a section of the Pioche Formation at Ruin Wash in eastern Nevada.

2.1. Emigrant Pass

At Emigrant Pass the Zabriskie Quartzite and Carrara Formation are easily accessible and well exposed. The strata are seen on the north side of Old Spanish Trail Highway as a continuous section of quartz arenite and shale forming slopes and moderately steep hillsides with limestone forming prominent ledges (Figs. 1 and 2). The Zabriskie Quartzite is dominated by burrowed and hummocky cross-bedded quartz arenite beds (Prave, 1991; Keller et al., 2012). It lacks age-diagnostic fossils, but rocks immediately above and below have yielded fauna from the *Bonnia-Olenellus* trilobite zone of Series 2 (Diehl, 1974; Palmer and Halley, 1979; Prave, 1991; Peng et al., 2012).

The Carrara Formation comprises cycles of silty marl and limestone with a trilobite fauna spanning the *Bonnia-Olenellus* to the *Glossopleura* zones, and thus the Series 2 - Series 3 boundary (Adams, 1995; Palmer and Halley, 1979; Sundberg and McCollum, 2000; Babcock et al., 2012; Keller et al., 2012; Fig. 3). The unit has been divided into nine members in the western Great Basin: Eagle Mountain Shale, Thimble Limestone, Echo Shale, Gold Ace Limestone, Pyramid Shale, Red Pass Limestone, Pahrump Hills Shale, Jangle Limestone and the Desert Range Limestone (Palmer and Halley, 1979). However, there is significant lateral variation within the Carrara Formation and at Emigrant Pass, the Thimble Limestone is not present (Palmer and Halley, 1979; Adams and Grotzinger, 1996). Overall the carbonate content of the Carrara Formation decreases in more basinward settings to the west (Hogan et al., 2011; Keller et al., 2012; Foster, 2014). Within the Carrara Formation at Emigrant Pass, five members are important to this study.

The Eagle Mountain Shale Member consists of green to grey-brown silty shale with interbedded lenses and beds of bioclastic limestone developed towards the top (Palmer and Halley, 1979). This is overlain by the Echo Shale Member which consists of green, platy shale and brown-orange limestone. The Echo Shale is correlated with the basal Combined Metals Member of the Pioche Formation in eastern Nevada (Palmer and Halley, 1979). The succeeding Gold Ace Limestone is a prominent, cliff-forming limestone (Cornwall and Kleinhampl, 1961). The strata include thin to medium-bedded lime mudstone, with dolomitic beds and oncolitic limestone (Palmer and Halley, 1979). Based on shared trilobite zones, the Gold Ace Limestone correlates with the Combined Metals Member of the Pioche Formation at Oak Springs Summit (Merriam and Palmer, 1964).

The overlying Pyramid Shale Member is a green shale with interbeds of brown and maroon silty marl and lenses of oncolitic and bioclastic limestone. Trilobite biostratigraphy indicates the Pyramid Shale is equivalent to two members of the Pioche Formation in eastern Nevada: the C-Shale Member and the Susan Duster Limestone Member (Palmer and Halley, 1979; Palmer, 1998). The Red Pass Limestone Member is the youngest unit examined in Death Valley. It forms prominent cliffs of oncolitic and bioclastic limestone, laminated lime mudstone and fenestral lime mudstone (Palmer and Halley, 1979). There is no equivalent limestone unit in the Pioche Formation of Nevada (Palmer and Halley, 1979).

2.2. Oak Springs Summit

At Oak Springs Summit, the Pioche Formation crops out to the west of a parking area in a dry river bed. Limestone forms more prominent ledges and platforms whilst shale forms recessively weathered outcrop (Figs. 1 and 2). The Combined Metals Member is composed of silty, oncolite-bearing dark limestone with *Olenellus* (Palmer, 1998; Sundberg and McCollum, 2000; Hollingsworth et al., 2011). It is overlain by the C- Shale Member (formerly the Comet Shale), a series of shale and thin-bedded limestone beds with pinch-and-swell bed boundaries (Palmer, 1998; Sundberg and McCollum, 2000). The Series 2 - Series 3 boundary is placed at the base of the C-Shale due to the sudden disappearance of the Olenellidae, and their replacement by a fauna dominated by *Eoptychoparia piochensis* at this level (Palmer, 1998; Sundberg and McCollum, 2000). The succeeding Susan Duster Limestone Member is a well-bedded, grey marl with occasional argillaceous and bioclastic limestone beds composed of trilobite fragments (Merriam and Palmer, 1964).

2.3. Biostratigraphy

Trilobite assemblages from the Carrara and Pioche formations belong to the *Olenellus*, *Eokochaspis nodosa*, *Amecephalus arrojosensis* and the *Plagiura-Poliella* zones that provide a framework for regional correlation (Merriam and Palmer, 1964; Palmer and Halley, 1979; Fig. 3). The *Olenellus* Zone ranges from the Zabriskie Quartzite to the basal portion of the Pyramid Shale Member within Death Valley (Palmer and Halley, 1979; Fig. 2). In Nevada, this zone spans the Delamar Member to the base of the C-Shale (Merriam and Palmer, 1964; Sundberg and McCollum, 2000). All olenellid trilobites disappear over a ~ 2 cm interval at the top of the zone, forming a distinct extinction horizon (Palmer, 1998; Fig. 2). This is immediately followed by first appearance of the ptychopariid trilobite *Eokochaspis nodosa*, which defines both the base of the *E. nodosa* Zone, and the Series 2 - Series 3 boundary (Sundberg and McCollum, 2000; Fig. 2). *E. nodosa* Zone faunas also occur in the Pyramid Shale Member in Death Valley (Sundberg and McCollum, 2000).

The succeeding *Amocephalus arrojosensis* Zone contains *A. arrojosensis*, *Mexicella robusta* and *Kochina? walcotti*. The zone is best defined at Hidden Valley, Nevada, where its base is 30 m above the base of the C-Shale Member (Merriam and Palmer, 1964), but it has not been recorded in the Carrara Formation due to a paucity of fossils above the *E. nodosoa* Zone in the Pyramid Shale (Palmer and Halley, 1979). However, trilobites, from the *Plagiura- Poliella* Zone, reappear in the uppermost Pyramid Shale and lower Red Pass Limestone (Palmer and Halley, 1979).

3. Methods

Sedimentary logging of the Carrara and Pioche formations was undertaken. At Emigrant Pass, 170 m of the Carrara Formation was logged from the base of the formation (at the contact with the Zabriskie Quartzite) up to the Red Pass Limestone Member. At Oak Springs Summit a 53 m-thick section of the Pioche Formation was logged, ranging from the basal Combined Metals Member to Susan Duster Limestone Member, an interval correlative with the Emigrant Pass section based on trilobite biostratigraphy (Merriam and Palmer, 1964; Palmer and Halley, 1979; Fig. 2). From these logs, four facies were defined (discussed below, Table 1). At the two study sections, 30 samples from the Pioche Formation and 57 samples from the Carrara Formation were analysed for $\delta^{13}C_{carb}$ (Table 2). In Lincoln County, Nevada, we also sampled the Ruin Wash location (Palmer, 1998; Lieberman, 2003) for additional facies and framboid analysis. Ruin Wash provided a second section (after Oak Springs Summit) where the extinction horizon of the olenellids is clearly seen (see Supplementary Material, Fig. S1). Facies analysis was undertaken in the field and complemented by petrographic examination of 49 thin sections. In order to evaluate redox conditions, pyrite framboid size distribution was also assessed on 21 samples using a scanning electron microscope (FEI Quanta 650 FEG-ESEM) in backscatter mode (see Bond and Wignall (2010) for procedure).

The calcite carbon (^{13}C / ^{12}C) and oxygen (^{18}O / ^{16}O) isotope values of powdered bulk sediment samples were measured on a total of 98 samples at the GeoZentrum Nordbayern, FAU Erlangen-Nurnberg, Germany (27 samples) and the School of Environmental Sciences, University of Liverpool, UK (71 samples). Carbon dioxide was prepared by reaction with phosphoric acid either at 70°C using a Gasbench II preparation system (FAU) or at 25 °C using the classical, 'sealed vessel' method (UoL). Mass ratios of the resultant purified gases were measured with a ThermoFisher Delta V plus mass spectrometer operating in continuous flow mode (FAU) or a VG SIRA 10 dual-inlet mass spectrometer (UoL). Raw gas data were corrected for ^{17}O effects and calibrated to the VPDB scale using a combination of international reference materials ($\delta^{13}C$ values are assigned as +1.95 ‰ to NBS 19 and –46.6 ‰ to LSVEC and $\delta^{18}O$ values of –2.20 ‰ to NBS19 and –23.2 ‰ to NBS18) and laboratory quality control materials and reported as conventional delta (δ) values. Analytical precision (1 σ) is estimated to be better than 0.1 ‰ for both isotope ratios based on replicate analysis of standards. Some notable differences in oxygen isotope values were reported where specific samples were duplicated by both laboratories. The reason for these differences is uncertain. Although some discrepancies were found to be significant, they do not impact on either the palaeoenvironmental or chemostratigraphic interpretation of the carbon isotope data.

The topmost 8 samples of the Carrara Formation were analysed at the University of Massachusetts, Amherst. Powdered, homogenized samples were analysed for $\delta^{13}C_{carb}$ and $\delta^{18}O_{carb}$ values using a Finnigan Delta XL+ isotope ratio mass spectrometer with an automated carbonate prep system (Kiel III). We report results as the per mille difference between sample and the VPDB standard in delta notation where $\delta^{18}O$ or $\delta^{13}C = (R_{sample} / R_{standard} - 1) \times 1000$, and R is the ratio of the minor to the major isotope. Results were calibrated using a house standard (crushed, washed and sieved marble) with VPDB values of +1.28 for $\delta^{13}C$ ‰ and –8.48 ‰ for $\delta^{18}O$. Reproducibility of standard materials is 0.1 ‰ for $\delta^{18}O$ and 0.05 ‰ for $\delta^{13}C$.

Total carbon (TC) and total organic carbon (TOC), following removal of calcite by acid decomposition of bulk sediment samples, was measured using a LECO SC-144DR Dual Range carbon and sulphur analyser at the University of Leeds. Total inorganic carbon (TIC) was subsequently calculated by difference (TIC = TC - TOC). An estimate of the calcite content for each sample was made by assuming that all TIC is hosted by calcite (wt % calcite = TIC x 8.333).

4. Results

4.1. Facies Analysis

Four facies and nine sub-facies were identified (Table 1): grainstone, packstone, silty marl and marl and they have been grouped into an onshore-offshore trend spanning shallow subtidal to outer shelf environments (Table 1). The shallowest strata consist of grainstone facies with common shell hash that is often abraded. Beds are typically decimetres thick and can show a hummocky top surface and sharp, erosive bases. Inclined stacks of flat-pebble intraclasts with herringbone-like cross stratification are present, suggesting storm wave processes (Fig. 4D). Bioturbated packstone, with sub-facies of oncolitic, bioclastic and silty packstone varieties (Fig. 5B), are interpreted to be a deeper facies based on the presence of a micritic mud matrix. Deeper water silty marl include fissile, homogenous and thoroughly bioturbated variants. Deepest-water, most offshore successions are dominated by fine grained marl, including sub-facies of laminated, pyritic dolomicrite and bioturbated marl with ichnofabric index (II) values of 2 - 3 (II2 and II3) in the scheme of Droser and Bottjer (1986).

The facies distribution reveals consistent trends in the two principal study sections. The base of the Carrara Formation, seen at Emigrant Pass, is dominated by deeper water facies (Facies 4) of the Eagle Mountain Shale. Commonly, the marl has a grey-green colour produced by the abundance of chlorite and clinochlore in the matrix (Figs. 4F, 5A and 6E). Laminated intervals are common, although these occur interbedded with burrowed strata suggesting there were frequent fluctuations of redox conditions.

The exception to the generally quiet, low-energy deposition of the Eagle Mountain Shale is recorded by a sharp, erosive-based bed of Facies 1 developed just over 30 m above the base of the section. This shelly, oncolitic packstone contains rip-up clasts of the underlying marl and sole marks on its base (Fig. 7A). Internally, thin intraclasts and shells display a chevron-stacking pattern (Fig. 4D). A major storm event seems likely to have produced this horizon with the shell-stacking produced by powerful bi-directional currents. The succeeding Echo Shale and Gold Ace members record shallowing. Grainstone and packstone dominate this 20-m-thick interval which includes erosive-based oncolitic packstone beds (Fig. 7B). Above this in the Pyramid Shale Member marl facies dominate, taken to be indicative of a sustained deepening. Grainstone and packstone facies developed in the lower ~ 15 m of the member are interpreted to have been transported during storm events. It is within this transgressive phase that the Series 2 - Series 3 boundary is recorded, along with the olenellid extinction (Foster, 2014). Deep-water sedimentation is abruptly terminated by the development of shallow-water grainstone at the base of the Red Pass Limestone Member (Fig. 7). Ooids and abraded fossil material (Table 1, Sub-Facies 1.1) suggest a nearshore setting.

The Pioche Formation at Oak Springs Summit records a more distal version of the succession seen within the Carrara Formation with relatively deep-water Facies 3 and 4 dominating (Fig. 2), though the same overall deepening-upwards trend is seen. Thus, the lower half of the Combined Metals Member consists of alternating silty marl and packstone. Above this, the remainder of the section is dominated by deeper-water facies (Fig. 2). The uppermost Combined Metals Member and the majority of the C-Shale Member record a similar transgressive deepening seen within the Pyramid Shale Member of the Carrara Formation. The olenellid extinction level occurs within this transgressive succession between a marl and a silty marl in the base of the C-Shale Member (Fig. 4E). This minor facies shift does not represent a significantly different environment and as such extinction is not thought to be a function of facies change. Immediately above the extinction horizon, chlorite in the form of both rounded grains and cement becomes common (Fig. 5A). The remainder of the C-Shale Member is a thick package of marl that transitions to silty marl at the base of the Susan Duster Limestone.

4.2. Pyrite Framboid Analysis

Framboid size analysis was performed on the Series 2 - Series 3 boundary strata (and thus the extinction horizon) from the Pioche Formation at Oak Springs Summit, where 11 samples were collected in a 7 m interval spanning 3.5 m either side of the extinction horizon. All samples contained abundant scattered crystals of pyrite ranging in size from 1-10 µm, often found agglomerated in clustered patches. Five samples yielded framboids preserved as iron oxyhydroxides due to weathering, with only minor amounts of original pyrite preserved in their core. The framboids showed a size distribution spanning an anoxic-dysoxic range (Fig. 8). The most dysoxic sample (smallest mean framboid diameter size and size range, lowest standard deviation) occurred in a marl approximately 1 m below the extinction horizon. Dysoxic framboid populations also occurred in the 1 m of strata overlying the extinction level. However, a sample from 20 cm below the extinction level did not yield any pyrite framboids suggesting fully oxygenated conditions. This variable degree of oxygen-restriction suggested by the framboid analysis is also seen in the variability of the associated sedimentary fabrics, which varies from laminated to slightly burrowed (II2).

Seven samples were also analysed from the Pioche Formation at Ruin Wash where the olenellid extinction horizon has been located within a succession of marls (Palmer, 1998; Lieberman, 2003; Fig. S1). Generally, framboidal pyrite was absent at this location with the exception of two samples from 10 and 15 cm below the extinction horizon where they had size ranges that plot in the anoxic field (Fig. 8). An additional four samples from around the extinction horizon at Emigrant Pass were also analysed. In this case, all samples only yielded scattered pyrite crystals but not framboids, suggesting better oxygenated conditions in this shallower-water section.

4.3. Chemostratigraphy

In the basal 20 m of the Carrara Formation $\delta^{13}C$ values are highly variable and do not show a clear trend (Fig. 7), but they then begin to stabilise around –2 ‰ before a consistent positive trend develops. In the Pyramid Shale Member the base of the negative excursion begins with at –0.1 ‰, above this $\delta^{13}C_{carb}$ values begin a decline to a lowpoint at 105 m of –3.5 ‰ (a negative shift of 3.4 ‰). In the overlying 25 m, no data was obtained because carbonate values were too low for analysis. Above this gap, $\delta^{13}C_{carb}$ values show a positive trend, returning to values around –0.1 ‰, similar to those from the base of the section.

Barring one outlier at the base of the section, $\delta^{13}C_{carb}$ values from the first 13 m of the Pioche Formation remain around –2.5 ‰ before there is a sharp, positive shift to –1.0 ‰ over the next 15 m (Fig. 7). From this value of –1.0 ‰ a negative shift occurs, resulting in peak negative values of –4.8 ‰. The nadir at the base of the C-Shale Member marks an overall shift of –3.8 ‰, a similar size to that found at Emigrant Pass. At the top of the section values return to around 0 ‰.

5. Discussion

5.1. Carbon isotopes and diagenesis

In order to evaluate the reliability of our isotope data we assess the preservation of a primary carbon isotope signal in our samples. In both the Carrara and Pioche formations the isotope analyses are derived from samples with a wide range of carbonate values (Table 2). The high TIC samples are likely to record primary carbon isotope signatures since they are buffered from external change by a large carbonate-carbon reservoir (Saltzman and Thomas, 2012). Lower TIC samples are more susceptible to post depositional isotopic alteration or addition of carbonate with a non-primary carbon isotope composition (Brand and Veizer, 1981; Banner and Hanson, 1990; Marshall, 1992). In both sections, the excursion to the lowest $\delta^{13}C_{carb}$ values occurs at the level of the trilobite extinction (mid-Pyramid Shale, Carrara Formation and basal C-Shale, Pioche Formation) where TIC is < 2 wt. %. Here we assess the preservation of a primary carbon isotope composition, particularly in samples with low TIC.

Two diagenetic processes can alter the primary isotopic composition: recrystallization of carbonate or precipitation of additional authigenic carbonate with a distinct isotope composition (Marshall, 1992). Both marine pore fluids and meteoric waters can have dissolved inorganic carbon (DIC) enriched in ^{12}C from the oxidation of organic matter and these mechanisms have differing predictions of the $\delta^{13}C_{carb}$ and $\delta^{18}O_{carb}$ values preserved (Marshall, 1992). Both the Carrara and Pioche formations display commonalities in their relationships between their $\delta^{13}C_{carb}$ and $\delta^{18}O_{carb}$ ratios and their TIC and TOC concentrations. Firstly (point 1), neither formation shows a clear relationship between $\delta^{13}C_{carb}$ and $\delta^{18}O_{carb}$ (Figs. S2 and S3). Secondly (point 2), samples with the most negative $\delta^{13}C_{carb}$ and the most positive $\delta^{18}O_{carb}$ are mostly characterised by low TIC (defined as < 2 wt. %). Both the Carrara and Pioche formations exhibit generally low TOC (point 3). In the Carrara Formation TOC concentrations range from 5.17 to 0.0 wt. % TOC with a mean concentration of 0.14 wt. % TOC. In the Pioche Formation concentrations range from 2.69 to 0.0 wt. % TOC, with a mean of

0.12 wt. % TOC. Finally (point 4), high TOC samples are characterised by more positive $\delta^{13}C_{carb}$. The major difference between the sections for these parameters is a much clearer positive relationship between TIC and $\delta^{13}C_{carb}$ within the Pioche Formation.

These observations rule out wholesale recrystallization in a meteoric fluid since neither section displays a positive correlation between $\delta^{18}O_{carb}$ and $\delta^{13}C_{carb}$ (point 1, Figs. S2 and S3). The generally low TOC concentrations and the relationship between TOC and $\delta^{13}C_{carb}$ (point 3 and 4) also makes localised precipitation of organic-carbon derived DIC doubtful. From the relationships between $\delta^{18}O_{carb}$ and TIC (point 2) it is likely that a proportion of the low TIC samples (< 2 wt. %) have undergone variable resetting of their $\delta^{18}O_{carb}$ towards more positive values. This observation is not consistent with precipitation of additional carbonate from unmodified meteoric or marine early diagenetic pore fluids, where the expectation would be a change towards more negative $\delta^{18}O_{carb}$ values (Marshall, 1992; Knauth and Kennedy, 2009; Cochran et al., 2010; Saltzman and Thomas, 2012). The remaining possibility to explain the oxygen isotope relationships is variable exchange with, or precipitation of carbonate from, a hypothetical high $\delta^{18}O$ fluid (Glumac and Walker, 1998). Since the climate at both sites is currently arid, one possibility is that the fluid in question is derived from evaporated modern meteoric water, but other possibilities exist (Saltzman and Thomas, 2012).

The relationships between $\delta^{13}C_{carb}$ and TIC differ somewhat from those between $\delta^{18}O_{carb}$ and TIC: from the Carrara Formation, the range of $\delta^{13}C_{carb}$ in the < 2 wt. % TIC samples overlaps strongly with the range found in near pure limestone samples suggesting that the influence of diagenetic process on $\delta^{13}C_{carb}$ at this site is likely to be minimal (Fig. S4). In contrast, samples from the Pioche Formation display a much clearer division between these two groups (TIC groups annotated in Fig. S5). This suggests that the influence of post-depositional process on $\delta^{13}C_{carb}$ may have been more pronounced at this site. However, the $\delta^{18}O_{carb}$ ranges of both high and low TIC samples of the Pioche Formation overlap (Fig. S6), indicating that at least some of the carbon isotope values have undergone minimal resetting.

In summary, there is clear evidence for a variable degree of oxygen isotope resetting towards more positive values, which is particularly pronounced in samples with low TIC (< 2 wt. %). There is also some evidence of concurrent variable resetting of carbon isotopes to more negative values in low TIC samples, with this being somewhat more pronounced in the Pioche Formation. Nonetheless, the presence of the negative $\delta^{13}C_{carb}$ values and the consistency of the magnitude of the excursion at level of the Series 2 - Series 3 boundary (e.g., Zhu et al., 2006; Faggetter et al., 2016), correlated independently by biostratigraphy between the two sections suggest that these samples record a predominantly primary signal. As such, we conclude that the negative $\delta^{13}C_{carb}$ excursion within the Carrara and Pioche formations preserves a primary record, given its co-occurrence with the olenellid extinction horizon, we interpret it to be ROECE.

5.2. Extinction and palaeoenvironmental change

Identification of the ROECE in the Pioche and Carrara formations (Fig. 7) confirms the close temporal relationship between trilobite extinctions and carbon isotope excursions (Zhu et al., 2006; Faggetter et al., 2016). It also allows examination of the associated facies and relative sea-level changes at this time. Initially the Sauk I/II supersequence boundary was placed around the Series 2 - Series 3 boundary (Sloss 1963). However, more recently this has been placed lower in the succession at the top of the Zabriskie Quartzite, underlying the Carrara Formation (Prave, 1991). Thus the Carrara Formation falls entirely within Sauk II (Keller et al., 2003, 2012; Morgan, 2012). Nonetheless, there are alternative regression surfaces in the Carrara Formation. A candidate for a sequence boundary occurs at the base of the Red Pass Limestone where there is a sharp transition from deep-water to shallow-water. This level lies around 45 m above ROECE in the Carrara Formation.

Rather than regression, the olenellid extinction occurs within a deepening succession. Transgression and shelf anoxia often go hand-in-hand, and oxygen stress has been implicated in ROECE extinction (Montañez et al., 2000). However, at Oak Springs Summit, pyrite framboid analysis suggests dysoxic but not euxinic conditions in the extinction interval, and the shallower study locations show no evidence for oxygen restriction. The evidence for intensified oxygen-restricted deposition at the trilobite extinction level is therefore weak. It also noteworthy that low-oxygen conditions were common in Cambrian oceans (Hurtgen et al., 2009; Pruss et al., 2010; Gill et al., 2011), and there is no suggestion that anoxia was intensified at the level of ROECE.

The Series 2 - Series 3 boundary interval saw the eruption of the Kalkarindji flood basalt province (Glass and Phillips, 2006; Jourdan et al., 2014; Marshall et al., 2016). In younger intervals of the Phanerozoic, the formation of large igneous provinces frequently coincides with mass extinctions (Wignall, 2015; Bond and Grasby, 2016) and the eruption of large volumes of volcanic volatiles provides a causal mechanism for driving biologic crises. The contemporaneous negative $\delta^{13}C$ signal of ROECE is often seen at times of LIP eruptions and may record the influx of isotopically-light volcanic CO_2 (e.g., Payne et al. 2004). Thus, in many regards the ROECE has the hallmarks of later Phanerozoic LIP-related mass extinctions although evidence for the commonly associated environmental changes such as the spread of anoxia (Wignall, 2015), is not clearly established for this Cambrian example.

6. Conclusions

In the western Great Basin, USA, the extinction of the dominant olenellid trilobites occurs within a deepening-upward shelf succession. A major –3.5‰ negative carbon isotope excursion (ROECE) occurs at the same level. This extinction/isotope event occurs around the Cambrian Series 2 - Series 3 boundary interval. Pyrite framboid size distribution data and laminated facies suggest periodic dysoxia occurred in the facies immediately surrounding the extinction horizon. However, these conditions were neither widespread (shallower-water boundary sections in Death Valley do not record oxygen starvation) nor especially unusual (laminated strata are sporadically developed throughout the offshore units of the Carrara Formation) suggesting dysoxia did not play a major role in the extinction. The environmental effects of the contemporaneous Kalkarindji flood basalt province of Australia provide a better potential causal for the extinction at the Series 2 - Series 3 boundary, although detailed correlation with the sections in North America is required.

Acknowledgments

We thank Emily Smith, Kristin Bergmann, and Jessica Creveling for valuable discussions in the field. We also thank Tessa Browne, along with Helena Tatgenhorst for allowing the use of their C isotope data in the top 25 m of Emigrant Pass, and Stephen Burns in the stable isotope laboratory at the University of Massachusetts at Amherst for providing these carbon isotope analyses. We thank an anonymous reviewer for their constructive feedback, and Jessica Creveling for her extensive and thorough review. This research was funded by a NERC postgraduate studentship to LEF.

Figure captions

Figure 1. Location map showing study sections at Emigrant Pass, Death Valley region, California (35° 53’ 29.24”N, 116° 04’ 39.08”W) and Oak Springs Summit, Burnt Spring Range, Lincoln County, Nevada (37°37’04.32”N 114°43’17.20”W). Star indicates approximate location of field area during the Cambrian Series 2 (after McKerrow et al., 1992).

Figure 2. Biostratigraphic correlation of the trilobite zones of the Carrara and Pioche formations (Palmer and Halley, 1979; Sundberg and McCollum, 2000). Facies column is based on field and petrographic observations, and numbers relate to facies detailed in Table 1. A generalised stratigraphic column of Precambrian and Cambrian formations in Death Valley is given (from Corsetti and Hagadorn, 2000).

Figure 3. Correlation of trilobite biozones within the Carrara and Pioche formations (Merriam and Palmer, 1965; Palmer and Halley, 1979; Sundberg and McCollum, 2000). *O.* is *Olenellus*, *P.* is *Poliella*.

Figure 4. Field photographs.

A. Trilobite debris (spines and carapaces and hyoliths) in a bioclastic hash on bedding planes of oolitic grainstone, Carrara Formation. B. Oncolitic packstone facies at Emigrant Pass. C. Bifurcating burrows in well bioturbated silty marl at Emigrant Pass, notebook for scale. D. Oolitic grainstone facies showing inclined chevron-style packing of thin intraclast and bioclasts (hyolith, ooid and other detrital fragments). E. Olenellid extinction level at the base of the C-Shale Member at Oak Springs Summit. Red line indicates extinction horizon from Palmer (1998). F. Fissile, laminated marl and silty marl in the lower Eagle Mountain Shale at Emigrant Pass. G. *Thalassinoides* in fine-grained, silty marl of the Carrara Formation. H. Vertical burrows (at the hammer tip) in silty marl beds of the Carrara Formation.

Figure 5. Scans of thin sections and photomicrographs.

A. Photomicrograph of a range of chlorite in the silty marl facies immediately above the extinction horizon at Oak Springs Summit. Chlorite occurs as elongate grains and also as cement. B: Photomicrograph of a silty bioclastic packstone in the upper Eagle Mountain Shale. C: Scan of slide of oncolitic packstone (Eagle Mountain Shale) showing oncoids with bioclastic nucleus of echinoderm plates amongst a matrix of shell detritus and micrite. D: Scan of slide of bioclastic grainstone. Elongate, trilobite fragments dominate this facies alongside hyolith remains and echinoderm plates. Dark brown mineral growth shows iron oxide preferentially replacing shell material.

Figure 6. Scans of thin sections and photomicrographs.

A: Scan of silty marl showing quartz grains and detrital chlorite grains (green). B: Photomicrograph of marl facies in the Combined Metals Member, Pioche Formation. Trilobite carapace exhibits brown needle like iron oxide replacement of the calcite shell. C: Photomicrograph of peloidal grainstone facies in the Combined Metals Member, Pioche Formation. Well rounded micrite pellets alongside rounded quartz grains amongst a fine micrite matrix. D: Photomicrograph of oolitic, bioclastic grainstone with iron oxides partially replacing ooids. E: Photomicrograph of silty chloritic limestone showing rounded chlorite grains (white dashed lines). F: Photomicrograph of chloritic silty marl facies showing sub-angular to angular quartz sand grains alongside hyolith and trilobite debris.

Figure 7. Carbon isotope chemostratigraphy of the Carrara Formation at Emigrant Pass and Pioche Formation at Oak Springs Summit. A. Inset log shows contact between silty micrite and an erosive-based oncolitic packstone with rip up clasts of the underlying silty micrite. This horizon grades laterally into an oolitic grainstone. B. Inset log of contact between silty bioclastic packstone and an erosive-based oncolitic packstone. Both erosional surfaces mark the transport of shallow water bioclastic material during storm events.

Figure 8. Size versus standard deviation for framboids from Series 2 - Series 3 boundary strata of California and Nevada showing the presence of oxygen-restricted facies. The threshold separating euxinic/anoxic and dysoxic/oxic size ranges in modern environments is from Wilkin et al. (1996).

Table 1: Facies of the Carrara and Pioche formations.

Table 2. Geochemical and framboid measurements for the Carrara and Pioche formations at Emigrant Pass (EP) and Oak Springs Summit (OSS) and framboid data from the Pioche Formation at Ruin Wash (RW).

References

Adams, R. D. (1995). Sequence-stratigraphy of Early-Middle Cambrian grand cycles in the Carrara Formation, southwest Basin and Range, California and Nevada. In *Sequence Stratigraphy and Depositional Response to Eustatic, Tectonic and Climatic Forcing* (pp. 277-328). Springer Netherlands.

Adams, R.D., Grotzinger, J. P. (1996). Lateral continuity of facies and parasequences in Middle Cambrian platform carbonates, Carrara Formation, southeastern California, USA. *Journal of Sedimentary Resesearch*, *66*(6), 1079-1090.

Banner, J.L., Hanson, G. N. (1990). Calculation of simultaneous isotopic and trace element variations during water-rock interaction with applications to carbonate diagenesis. *Geochim. Cosmo. Acta 54*(11), 3123-3137.

Bond, D.P.G., Grasby, S.E. (2016). On the causes of mass extinctions. *Palaeogeography, Palaeoclimatology, Palaeoecology. (In this issue).*

Bond, D.P.G, Wignall, P.B. (2010). Pyrite framboid study of marine Permian-Triassic boundary sections: a complex anoxic event and its relationship to contemporaneous mass extinction. *Geological Society of America Bulletin*, *122*(7-8), 1265-1279.

Bond, G. C., and Kominz, M. A. (1984). Construction of tectonic subsidence curves for the early Paleozoic miogeocline, southern Canadian Rocky Mountains: Implications for subsidence mechanisms, age of breakup, and crustal thinning. *Geological Society of America Bulletin*, *95*(2), 155-173.

Boucot, A. J. (1990). Phanerozoic extinctions: How similar are they to each other? In *Extinction Events in Earth History* (pp. 5-30). Springer Berlin Heidelberg.

Brand, U., Veizer, J. (1981). Chemical diagenesis of a multicomponent carbonate system-2: stable isotopes. *Journal of Sedimentary Petrology*, *51*(3), 987-997.

Cochran, J. K., Kallenberg, K., Landman, N. H., Harries, P. J., Weinreb, D., Turekian, K. K., Cobban, W. A. (2010). Effect of diagenesis on the Sr, O, and C isotope composition of late Cretaceous mollusks from the Western Interior Seaway of North America. *American Journal of Science*, *310*(2), 69-88.

Cornwall, H. R., Kleinhampl, F. J. (1961). Geology of the Bare Mountain Quadrangle, Nevada. USGS Report No. 157.

Corsetti, F. A., and Hagadorn, J. W. (2000). Precambrian-Cambrian transition: Death Valley, United States. Geology, 28(4), 299-302.

Debrenne, F. (1991). Extinction of the Archaeocyatha. *Historical Biology*, 5 (2-4), 95-106.

Diehl, P. E. (1974). Stratigraphy and sedimentology of the Wood Canyon Formation, Death Valley area, California. *Death Valley Region, California and Nevada, Geol Soc Am, Cordilleran Section Annual Meeting, 70th, Las Vegas, Nevada, 1974, Guidebook, p.* 37-48.

Droser, M.L., Bottjer, D.J. (1986). A semiquantitative field classification of ichnofabric: research method paper. *Journal of Sedimentary Research*, *56*(4), 558-559.

Erdtmann, B.D., Miller, J.F. (1981). Eustatic control of lithofacies and biofacies changes near the base of the Tremadocian. In *Short Papers for the Second International Symposium on the Cambrian System. USGS Open-File Report,* 81-743, 78-81.

Faggetter, LE., Wignall, P.B., Pruss, S.B., Sun, Y., Raine, R.J., Newton, R.J., Widdowson, M., Joachimski, M.M., Smith, P.M. (2016). Sequence stratigraphy, chemostratigraphy and facies analysis of Cambrian Series 2 - Series 3 boundary strata in northwest Scotland. *Geological Magazine*, pp. 1-13

Fan, R., Deng, S., Zhang, X. (2011). Significant carbon isotope excursions in the Cambrian and their implications for global correlations. *Science China Earth Sciences*, 54(11), 1686-1695.

Fedo, C.M., Cooper, J.D. (2001). Sedimentology and sequence stratigraphy of Neoproterozoic and Cambrian units across a craton-margin hinge zone, southeastern California, and implications for the early evolution of the Cordilleran margin. *Sedimentary Geology*, *141*, 501-522.

Foster, J. (2014). *Cambrian ocean world: ancient sea life of North America*. Indiana University Press, 432 pp.

Gill, B.C., Lyons, T.W., Young, S.A., Kump, L.R., Knoll, A.H., Saltzman, M.R. (2011). Geochemical evidence for widespread euxinia in the Later Cambrian ocean. *Nature*, *469*(7328), 80-83.

Glass, L.M., Phillips, D. (2006). The Kalkarindji continental flood basalt province: a new Cambrian large igneous province in Australia with possible links to faunal extinctions. *Geology*, *34*(6), 461-464.

Glumac, B., Walker, K.R. (1998). A Late Cambrian positive carbon-isotope excursion in the southern Appalachians: Relation to biostratigraphy, sequence stratigraphy, environments of deposition, and diagenesis. *Journal of Sedimentary Research*, *68*(6), 1212-1222

Hallam, A., Wignall, P.B. (1997). *Mass extinctions and their aftermath*. Oxford University Press, Oxford, 320pp.

Hollingsworth, J.S., Sundberg, F.A., Foster, J.R. (2011). Cambrian stratigraphy and paleontology of Northern Arizona and Southern Nevada. *Museum of Northern Arizona Bulletin*, *67*, 321.

Hogan, E.G., Fedo, C.M., Cooper, J.D. (2011). Reassessment of the basal Sauk Supersequence boundary across the Laurentian craton-margin hinge zone, southeastern California. *The Journal of Geology*, *119*(6), 661-685.

Howley, R.A., Rees, M. N., Jiang, G. (2006). Significance of Middle Cambrian mixed carbonate-siliciclastic units for global correlation: southern Nevada, USA. *Palaeoworld*, *15*(3), 360-366.

Hurtgen, M.T., Pruss, S. B., Knoll, A. H. (2009). Evaluating the relationship between the carbon and sulfur cycles in the later Cambrian ocean: an example from the Port au Port Group, western Newfoundland, Canada. *Earth and Planetary Science Letters*, *281*(3), 288-297.

Jourdan, F., Hodges, K., Sell, B., Schaltegger, U., Wingate, M.T. D., Evins, L.Z., Blenkinsop, T. (2014). High-precision dating of the Kalkarindji large igneous province, Australia, and synchrony with the Early-Middle Cambrian (Stage 4-5) extinction. *Geology*, *42*(6), 543-546.

Keller, M., Cooper, J., Lehnert, O. (2003). Sauk sequence sequences (southern Great Basin) [abstract]. In: Geological Society of American *Abstracts with Programs,* Vol. 35, No.6, September 2003, p.543

Keller, M., Cooper, J.D., Lehnert, O. (2012). Sauk megasequence supersequences, southern Great Basin: Second-order accommodation events on the southwestern Cordilleran margin platform, in J.R. Derby, R.D. Fritz, S.A. Longacre, W.A. Morgan, and C.A. Sternbach, eds., *The great American carbonate bank: The geology and economic resources of the Cambrian- Ordovician Sauk megasequence of Laurentia*: AAPG Memoir 98, p. 873- 896

Knauth, L.P., Kennedy, M.J. (2009). The late Precambrian greening of the Earth. *Nature*, *460*(7256), 728-732.

Landing, Ed, (2012). The great American carbonate bank in eastern Laurentia: Its births, deaths, and linkage to paleooceanic oxygenation (Early Cambrian - Late Ordovician), in J. R. Derby, R. D. Fritz, S. A. Longacre, W. A. Morgan, and C. A. Sternbach, eds., *The great American carbonate bank: The geology and economic resources of the Cambrian - Ordovician Sauk megasequence of Laurentia*: AAPG Memoir 98, p. 451 - 492.

Levy, M., Christie-Blick, N. (1991). Tectonic subsidence of the early Paleozoic passive continental margin in eastern California and southern Nevada. *Geological Society of America Bulletin*, *103*(12), 1590-1606.

Lieberman, B.S. (2003). A new soft-bodied fauna: the Pioche Formation of Nevada. *Journal of Paleontology*, *77*(04), 674-690.

MacNiocaill, C., Smethurst, M.A. (1994). Palaeozoic palaeogeography of Laurentia and its margins: a reassessment of palaeomagnetic data.*Geophysical Journal International*, *116*(3), 715-725.

Marshall, J.D. (1992). Climatic and oceanographic isotopic signals from the carbonate rock record and their preservation. *Geological magazine*, *129*(02), 143-160.

Marshall, P.E., Widdowson, M., Murphy, D. T. (2016). The giant lavas of Kalkarindji: rubbly pāhoehoe lava in an ancient continental flood basalt province. *Palaeogeography, Palaeoclimatology, Palaeoecology*, *441*, 22-37.

McKerrow, W.S., Scotese, C.R., Brasier, M.D. (1992). Early Cambrian continental reconstructions. *Journal of the Geological Society, 149(4),* 599-606.

Merriam, C.W., Palmer, A.R. (1964*).* Cambrian rocks of the Pioche mining district, Nevada, with a section on Pioche shale faunules (No. 469). *USGS Professional Paper, 264*-D, 53-86

Montañez, I.P., Osleger, D. A., Banner, J.L., Mack, L. E., Musgrove, M. (2000). Evolution of the Sr and C isotope composition of Cambrian oceans. *GSA today*, *10*(5), 1-7.

Morgan, W.A. (2012). Sequence stratigraphy of the great American carbonate bank, *in,* Derby, J.R., Fritz, R.D., Longacre, S.A., Morgan, W.A., and Sternbach, C.A., eds., The Great American Carbonate Bank: The Geology and Economic Resources of the Cambrian-Ordovician Sauk Megasequences of Laurentia: Association of American Petroleum Geologists Memoir 98, p.37-79.

Newell, N.D. (1972). The evolution of reefs. *Scientific American*, 226, 54-65.

Palmer, A.R., Halley, R.B. (1979). Physical stratigraphy and trilobite biostratigraphy of the Carrara Formation (Lower and Middle Cambrian) in the southern Great Basin. *USGS Professional Paper,* No.1047*.*

Palmer, A. R. (1984). The biomere problem: evolution of an idea. *Journal of Paleontology*, 599-611.

Palmer, A.R. (1998). Terminal early Cambrian extinction of the Olenellina: documentation from the Pioche Formation, Nevada. *Journal of Paleontology*, 72 (04), 650-672.

Payne, J.L., Lehrmann, D.J., Wei, J., Orchard, M. J., Schrag, D. P., Knoll, A.H. (2004). Large perturbations of the carbon cycle during recovery from the end-Permian extinction. *Science*, *305*(5683), 506-509.

Peng, S., Babcock, L.E., Cooper, R.A. (2012). The Cambrian Period. . In: Gradstein, F., Ogg, J., Schmitz, M., Ogg, G. (Eds). *The Geologic Time Scale* 2012, Elsevier, Boston, 2, 437-488.

Prave, A.R. (1991). Depositional and sequence stratigraphic framework of the Lower Cambrian Zabriskie Quartzite: implications for regional correlations and the Early Cambrian paleogeography of the Death Valley region of California and Nevada. *Geological Society of America Bulletin*, 104(5), 505-515.

Prave, A. R. (1999). Two diamictites, two cap carbonates, two δ13C excursions, two rifts: the Neoproterozoic Kingston Peak Formation, Death Valley, California. *Geology*, 27(4), 339-342.

Pruss, S.B., Finnegan, S., Fischer, W.W., Knoll, A.H. (2010). Carbonates in skeleton-poor seas: new insights from Cambrian and Ordovician strata of Laurentia. *Palaios*, *25*(2), 73-84.

Saltzman, M.R., Thomas, E. (2012). Chapter 11- Carbon isotope stratigraphy. In: Gradstein, F., Ogg, J., Schmitz, M., Ogg, G. (Eds). *The Geologic Time Scale* 2012, Elsevier, Boston, *1*, 207-232.

Saltzman, M.R., Edwards, C.T., Adrain, J.M., Westrop, S.R. (2015). Persistent oceanic anoxia and elevated extinction rates separate the Cambrian and Ordovician radiations. *Geology*, *43*(9), 807-810.

Sloss, L.L. (1963). Sequences in the cratonic interior of North America. Geological Society of America Bulletin, 74(2), 93-114.

Stewart, J. H. (1972). Initial deposits in the Cordilleran geosyncline: Evidence of a late Precambrian (< 850 my) continental separation. *Geological Society of America Bulletin*, *83*(5), 1345-1360.

Sundberg, F.A., McCollum, L.B. (2000). Ptychopariid trilobites of the lower-middle Cambrian boundary interval, Pioche Shale, southeastern Nevada*. Journal of Paleontology*, 74(4), 604-630.

Sundberg, F. A., Geyer, G., Kruse, P. D., McCollum, L. B., Pegel, T. V., Zylinska, A., Zhuravlev, A. Y. (2016). International correlation of the Cambrian Series 2 - 3, stages 4 - 5 boundary interval. *Australasian Palaeontological Memoirs*, 49, 83-124

Tarhan, L. G., Droser, M.L., Planavsky, N. J., Johnston, D.T. (2015). Protracted development of bioturbation through the early Palaeozoic Era. *Nature Geoscience*, 8, 865-869.

Wang, X., Hu, W., Yao, S., Chen, Q., Xie, X. (2011). Carbon and strontium isotopes and global correlation of Cambrian Series 2 - Series 3 carbonate rocks in the Keping area of the northwestern Tarim Basin, NW China. *Marine and Petroleum Geology*, 28(5), 992-1002.

Wignall, P.B. (2001). Large igneous provinces and mass extinctions. *Earth-Science Reviews*, 53(1), 1-33.

Wignall, P.B. (2015). *The Worst of Times: How Life on Earth Survived Eighty Million Years of Extinctions*. Princeton University Press.

Wilkin, R. T., Barnes, H. L., Brantley, S.L. (1996). The size distribution of framboidal pyrite in modern sediments: an indicator of redox conditions. *Geochimica et Cosmochimica Acta*, *60*(20), 3897-3912.

Zhang, W., Shi, X., Jiang, G., Tang, D., Wang, X. (2013). Mass-occurrence of oncoids at the Cambrian Series 2 - Series 3 transition: Implications for microbial resurgence following an Early Cambrian extinction*. Gondwana Research*, 28(1), 432-450.

Zhu, M. Y., Zhang, J. M., Li, G. X., Yang, A. H. (2004). Evolution of C isotopes in the Cambrian of China: implications for Cambrian subdivision and trilobite mass extinctions. *Geobios*, 37(2), 287-301.

Zhu, M.Y., Babcock, L.E., Peng, S.C. (2006). Advances in Cambrian stratigraphy and paleontology: integrating correlation techniques, paleobiology, taphonomy and paleoenvironmental reconstruction. *Palaeoworld*, 15(3), 217-222.

Zhuravlev, A.Y., Wood, R. A. (1996). Anoxia as the cause of the mid-Early Cambrian (Botomian) extinction event. *Geology*, 24(4), 311-314.

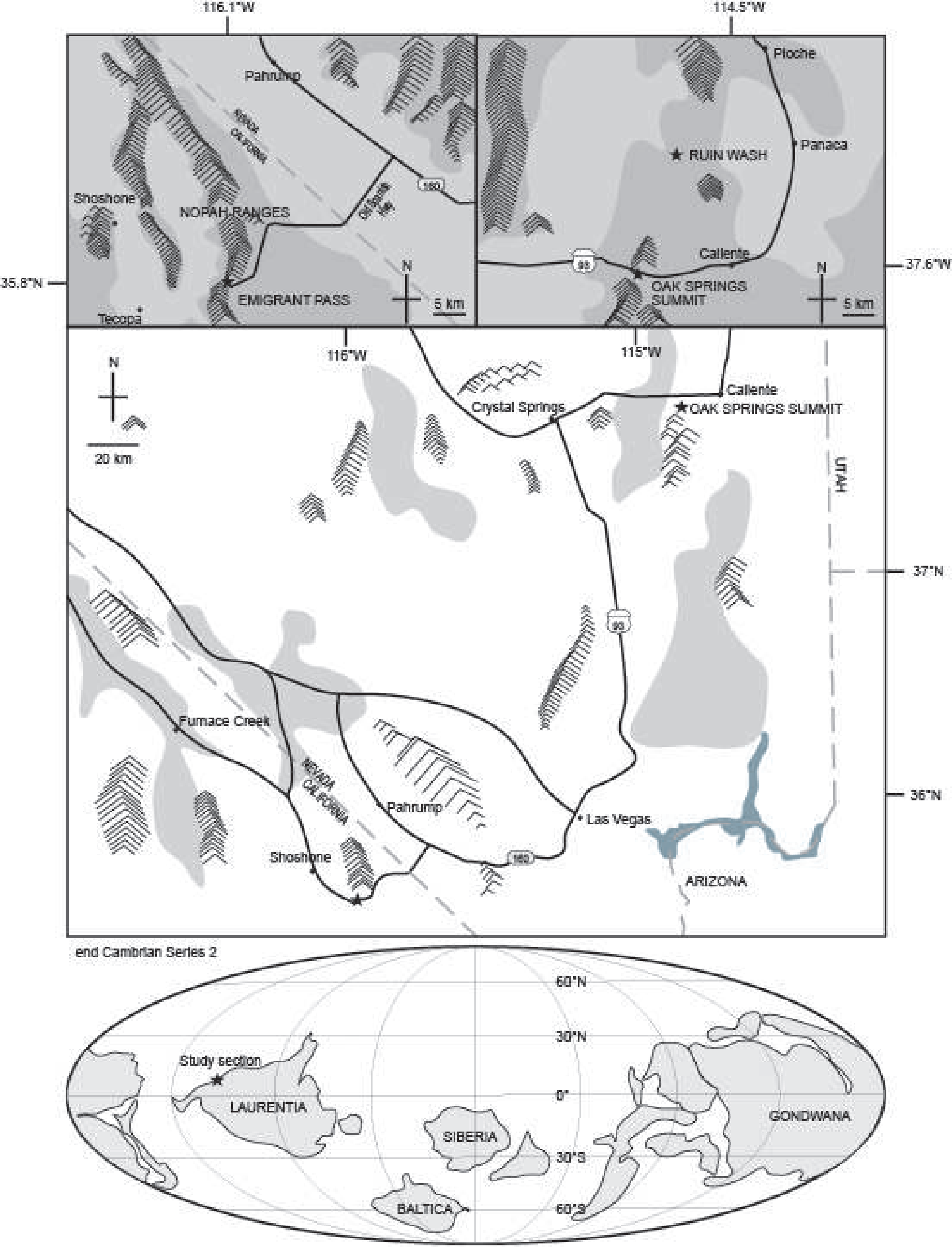
116.1°W
114.5°W
Pahrump
Shoshone
NOPAH RANGES
EMIGRANT PASS
Tecopa
35.8°N
5 km
160
Pioche
Panaca
RUIN WASH
Caliente
93
OAK SPRINGS SUMMIT
37.6°N
5 km
116°W
115°W
20 km
Crystal Springs
Caliente
OAK SPRINGS SUMMIT
UTAH
37°N
93
Furnace Creek
NEVADA
CALIFORNIA
Pahrump
Shoshone
Las Vegas
160
36°N
ARIZONA
end Cambrian Series 2
60°N
30°N
0°
30°S
60°S
Study section
LAURENTIA
SIBERIA
BALTICA
GONDWANA

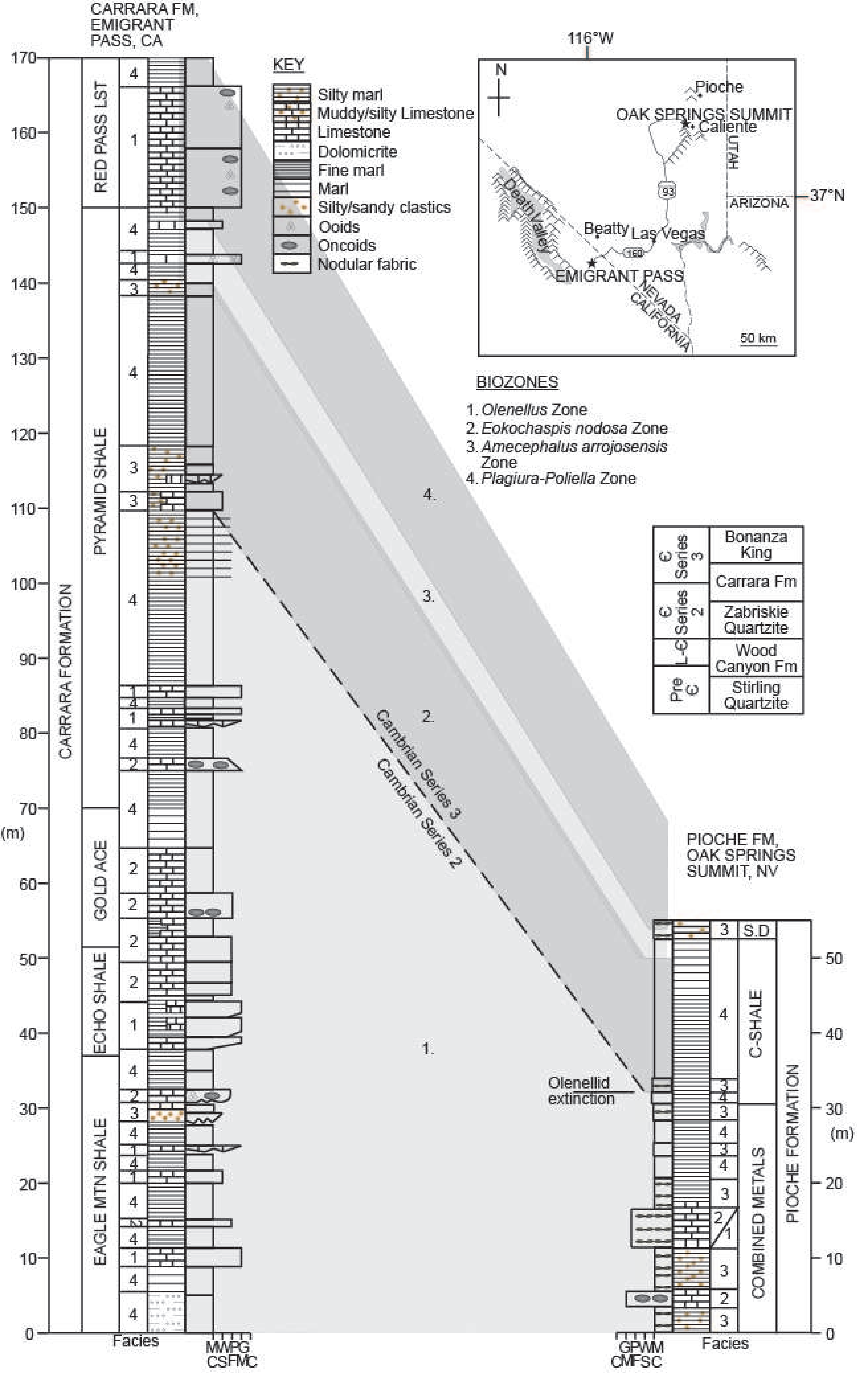

CARRARA FM, EMIGRANT PASS, CA
KEY
Silty marl
Muddy/silty Limestone
Limestone
Dolomicrite
Fine marl
Marl
Silty/sandy clastics
Ooids
Oncoids
Nodular fabric
116°W
N
Pioche
OAK SPRINGS SUMMIT
Caliente
UTAH
93
37°N
ARIZONA
Death Valley
Beatty
Las Vegas
160
EMIGRANT PASS
NEVADA
CALIFORNIA
50 km
BIOZONES
1. Olenellus Zone
2. Eokochaspis nodosa Zone
3. Amecephalus arrojosensis Zone
4. Plagiura-Poliella Zone
Є Series 3
Є Series 2
L-Є
Pre Є
Bonanza King
Carrara Fm
Zabriskie Quartzite
Wood Canyon Fm
Stirling Quartzite
CARRARA FORMATION
RED PASS LST
PYRAMID SHALE
GOLD ACE
ECHO SHALE
EAGLE MTN SHALE
(m)
Cambrian Series 3
Cambrian Series 2
PIOCHE FM, OAK SPRINGS SUMMIT, NV
Olenellid extinction
S.D
C-SHALE
COMBINED METALS
PIOCHE FORMATION
Facies
MWPG
CSFMC
GPWM
CMFSC

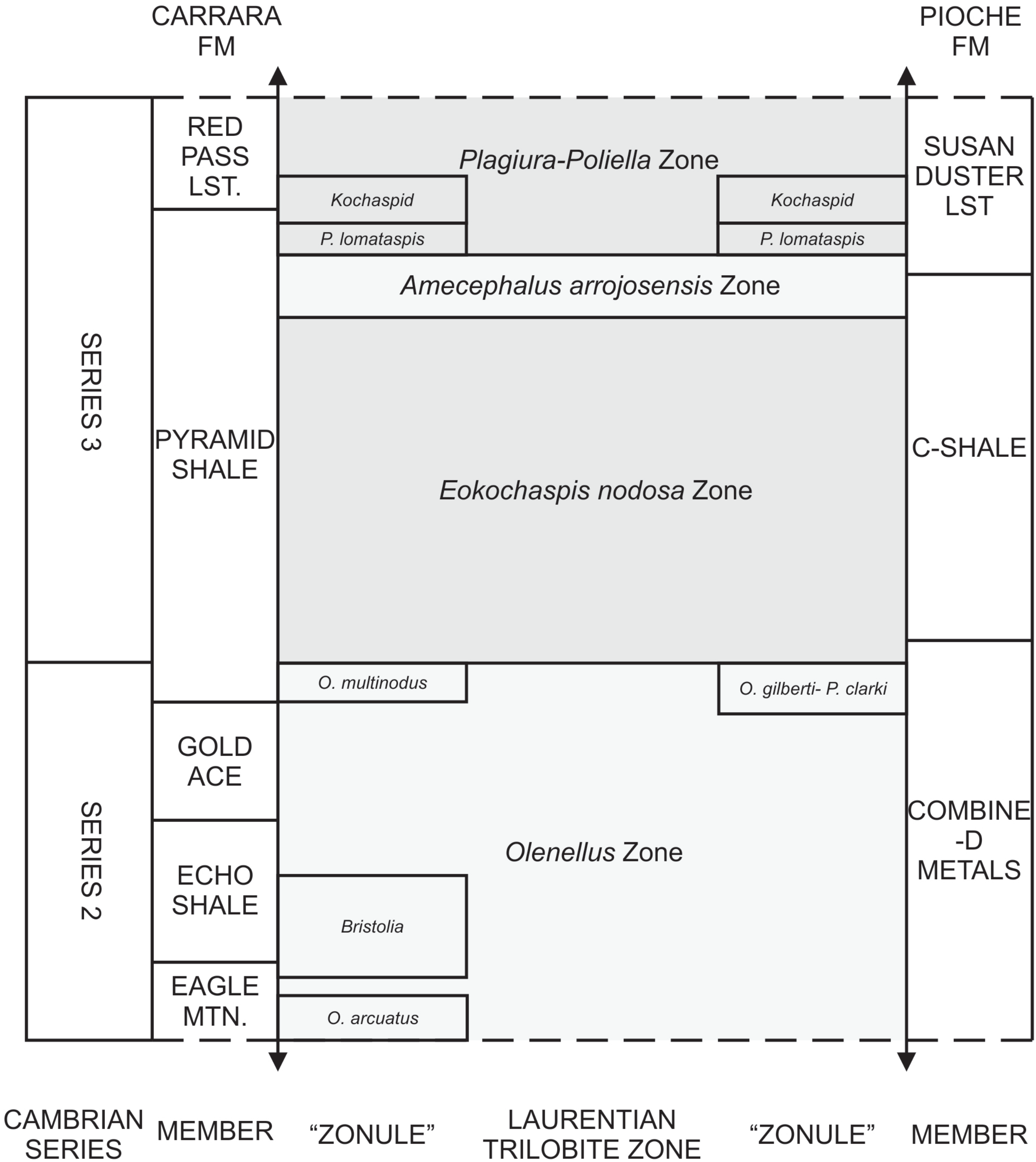
CARRARA FM
PIOCHE FM
RED PASS LST.
PYRAMID SHALE
GOLD ACE
ECHO SHALE
EAGLE MTN.
SERIES 3
SERIES 2
Plagiura-Poliella Zone
Kochaspid
P. lomataspis
Amecephalus arrojosensis Zone
Eokochaspis nodosa Zone
O. multinodus
O. gilberti- P. clarki
Olenellus Zone
Bristolia
O. arcuatus
SUSAN DUSTER LST
C-SHALE
COMBINE-D METALS
CAMBRIAN SERIES
MEMBER
"ZONULE"
LAURENTIAN TRILOBITE ZONE
"ZONULE"
MEMBER

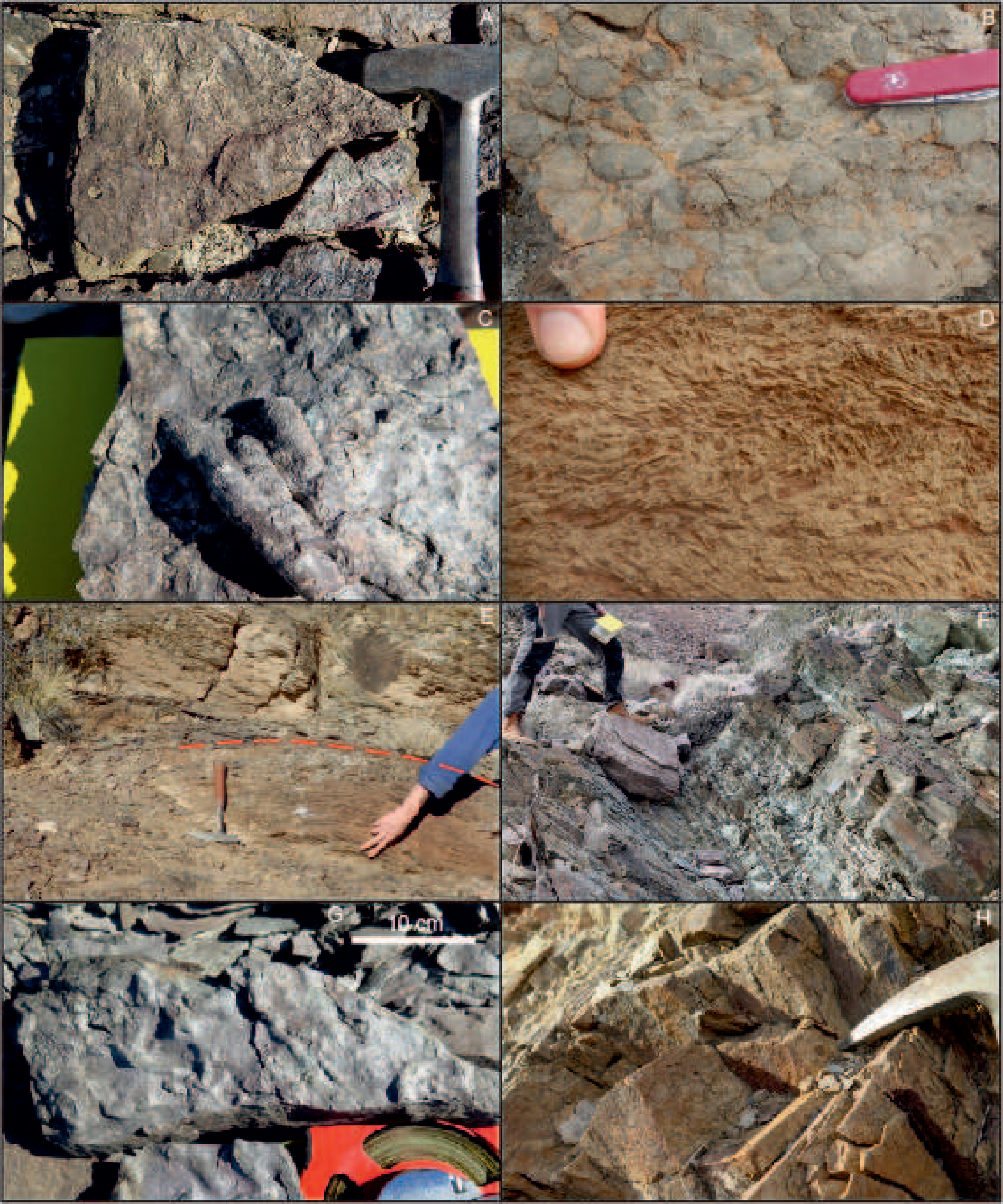
A
B
C
D
E
F
G
10 cm
H

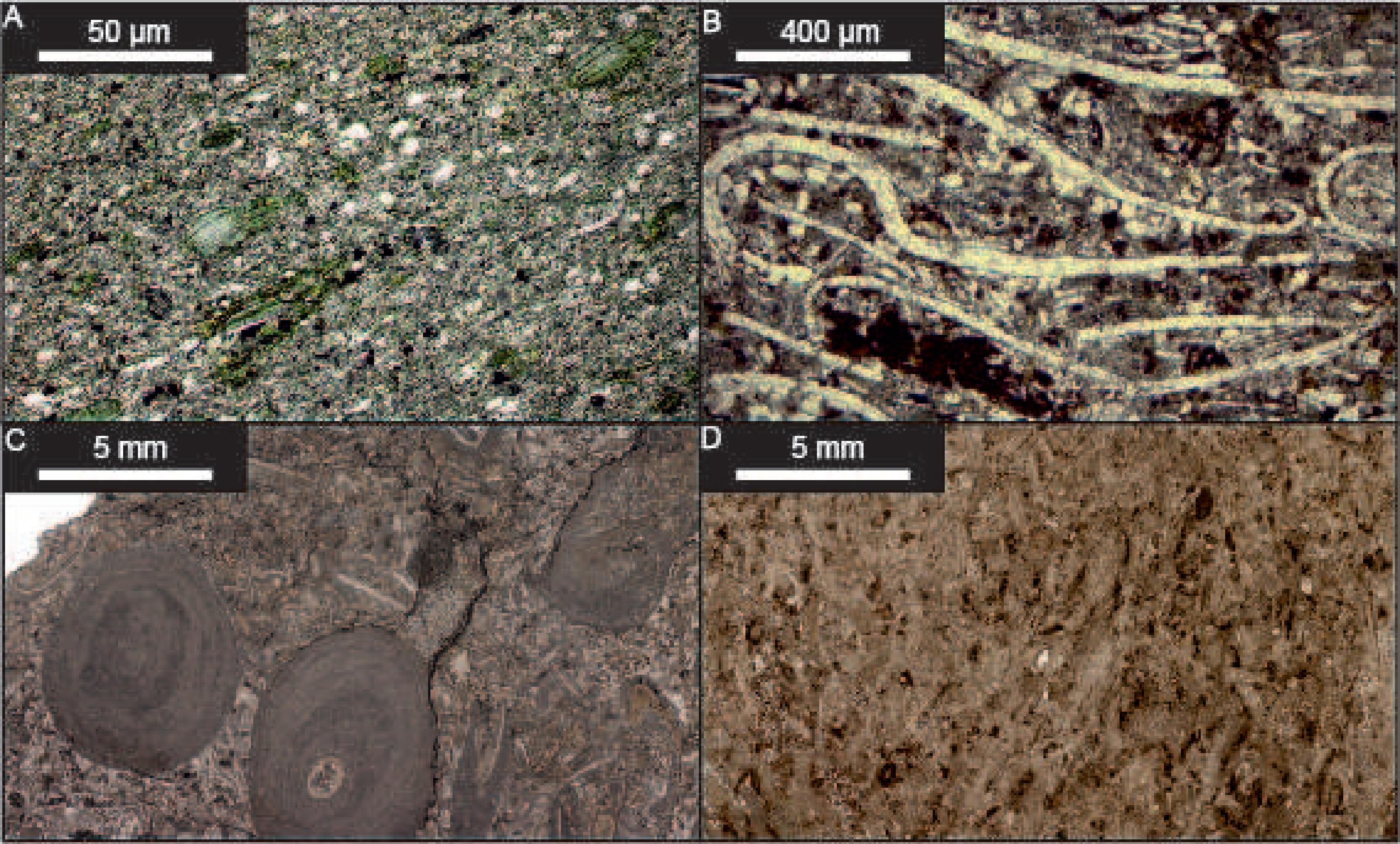
A
50 μm
B
400 μm
C
5 mm
D
5 mm

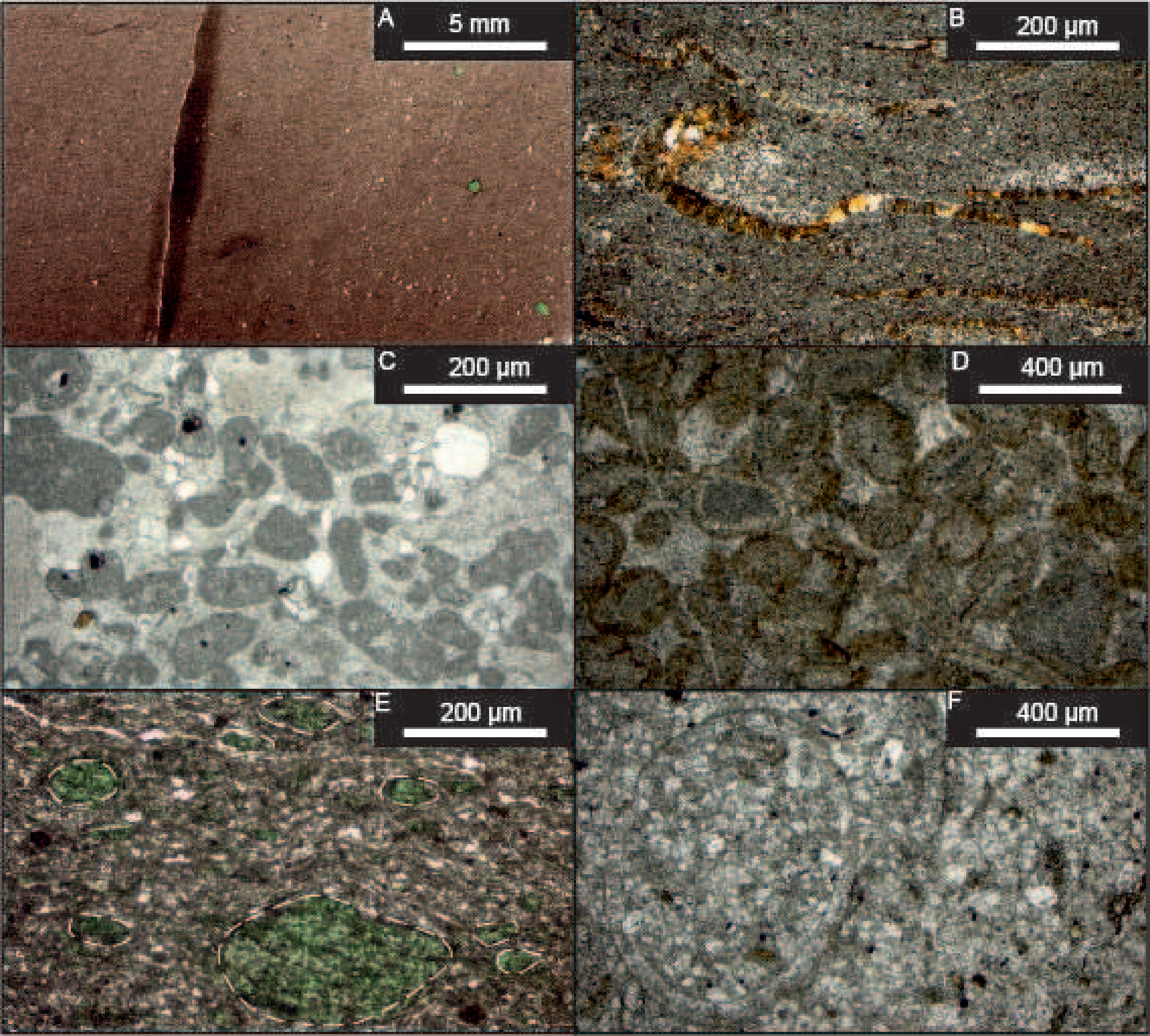
A
5 mm
B
200 µm
C
200 µm
D
400 µm
E
200 µm
F
400 µm

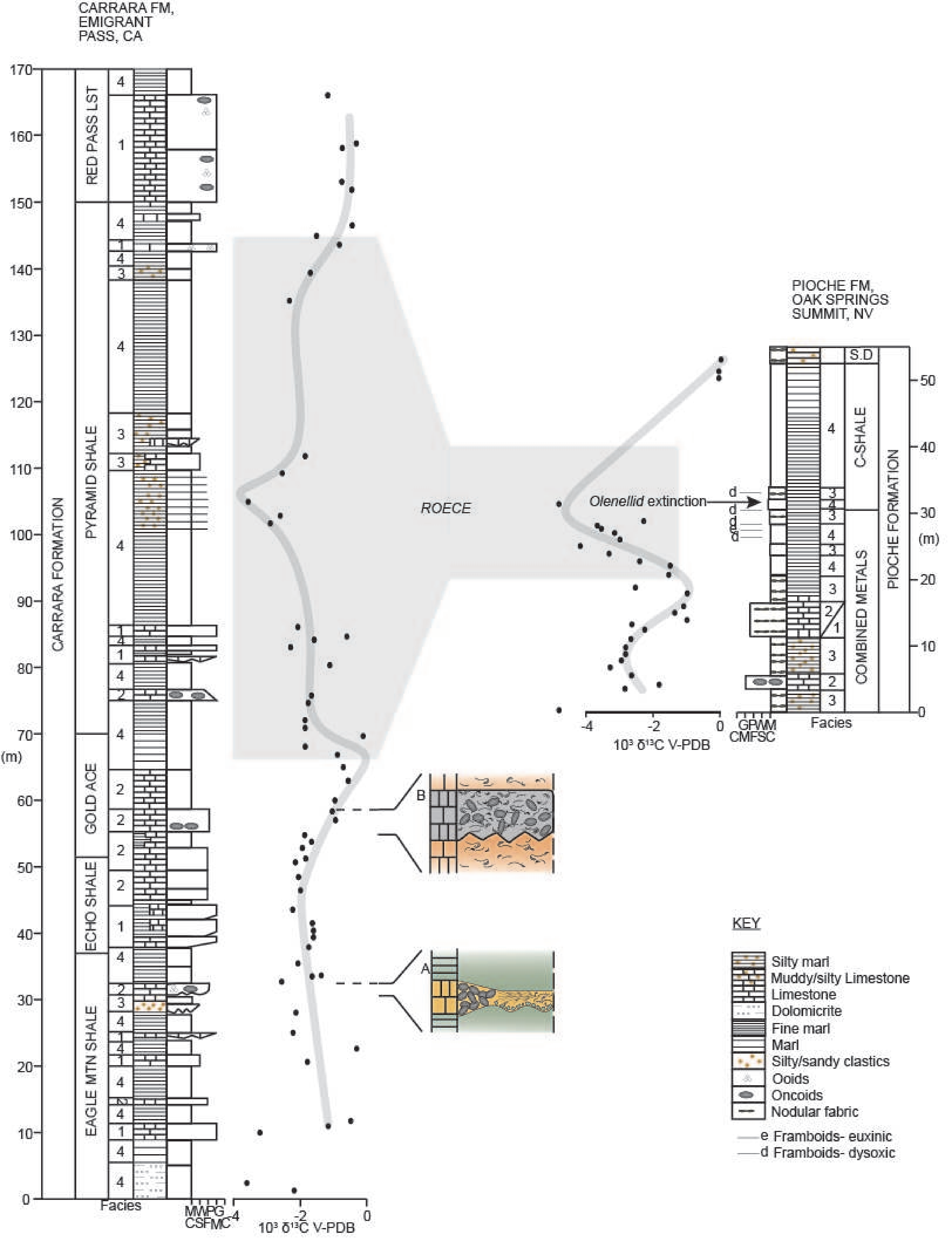
CARRARA FM, EMIGRANT PASS, CA
CARRARA FORMATION
RED PASS LST
PYRAMID SHALE
GOLD ACE
ECHO SHALE
EAGLE MTN SHALE
(m)
Facies
MWPG
CSFMC
10³ δ¹³C V-PDB
ROECE
A
B
PIOCHE FM, OAK SPRINGS SUMMIT, NV
Olenellid extinction
S.D
C-SHALE
COMBINED METALS
PIOCHE FORMATION
GPWM
CMFSC
KEY
Silty marl
Muddy/silty Limestone
Limestone
Dolomicrite
Fine marl
Marl
Silty/sandy clastics
Ooids
Oncoids
Nodular fabric
e Framboids- euxinic
d Framboids- dysoxic

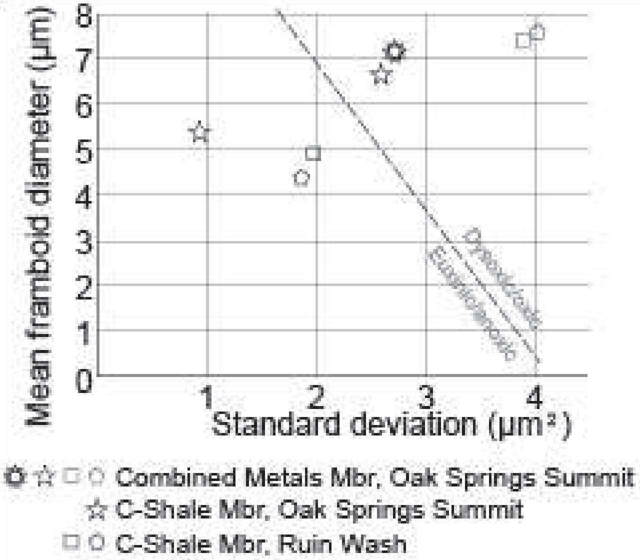
Mean framboid diameter (µm)
0
1
2
3
4
5
6
7
8
1
2
3
4
Standard deviation (µm²)
Dysoxic/oxic
Euxinic/anoxic
Combined Metals Mbr, Oak Springs Summit
C-Shale Mbr, Oak Springs Summit
C-Shale Mbr, Ruin Wash

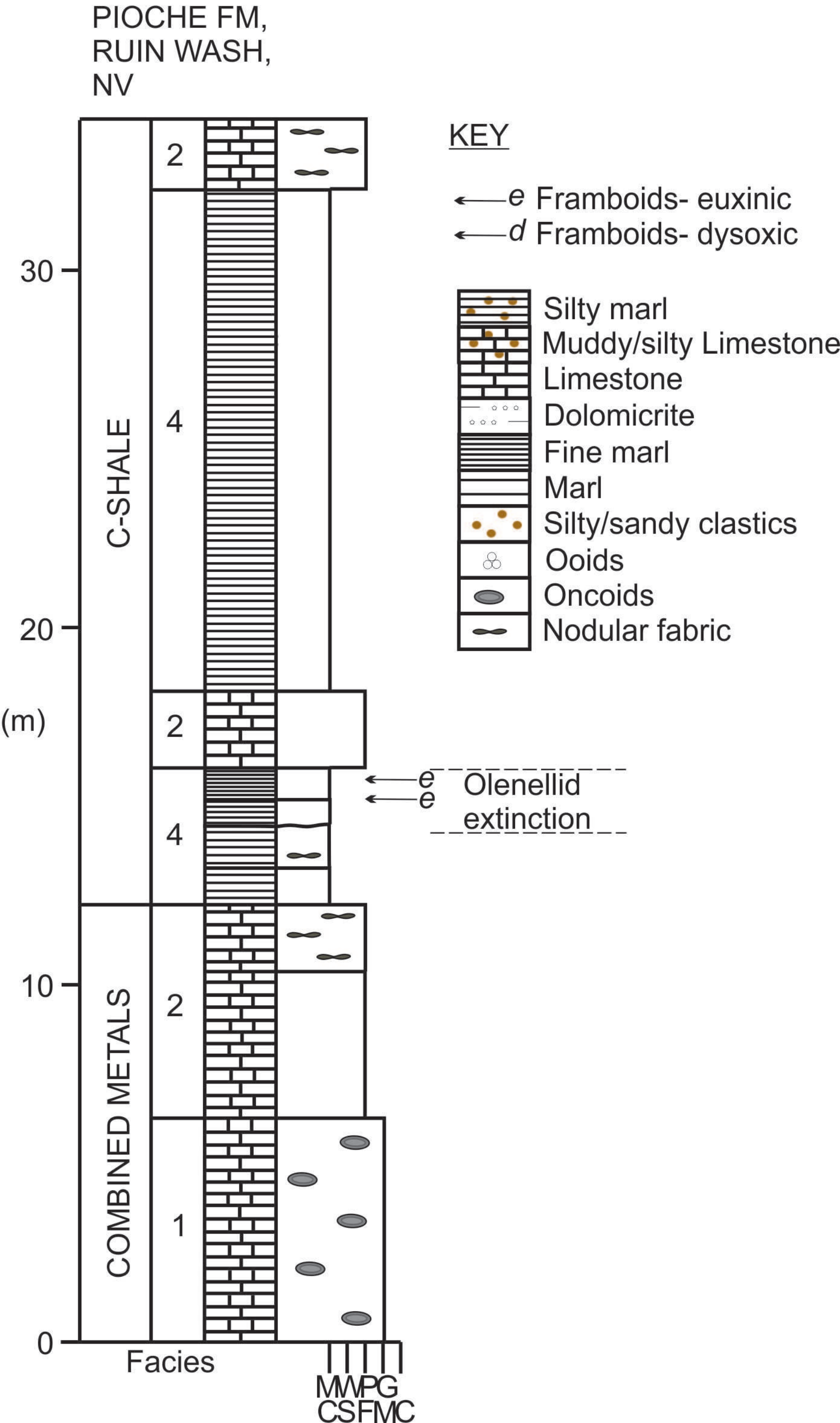
PIOCHE FM, RUIN WASH, NV
KEY
e Framboids- euxinic
d Framboids- dysoxic
Silty marl
Muddy/silty Limestone
Limestone
Dolomicrite
Fine marl
Marl
Silty/sandy clastics
Ooids
Oncoids
Nodular fabric
30
20
(m)
10
0
C-SHALE
COMBINED METALS
2
4
2
4
2
1
e
e
Olenellid extinction
Facies
MWPG
CSFMC

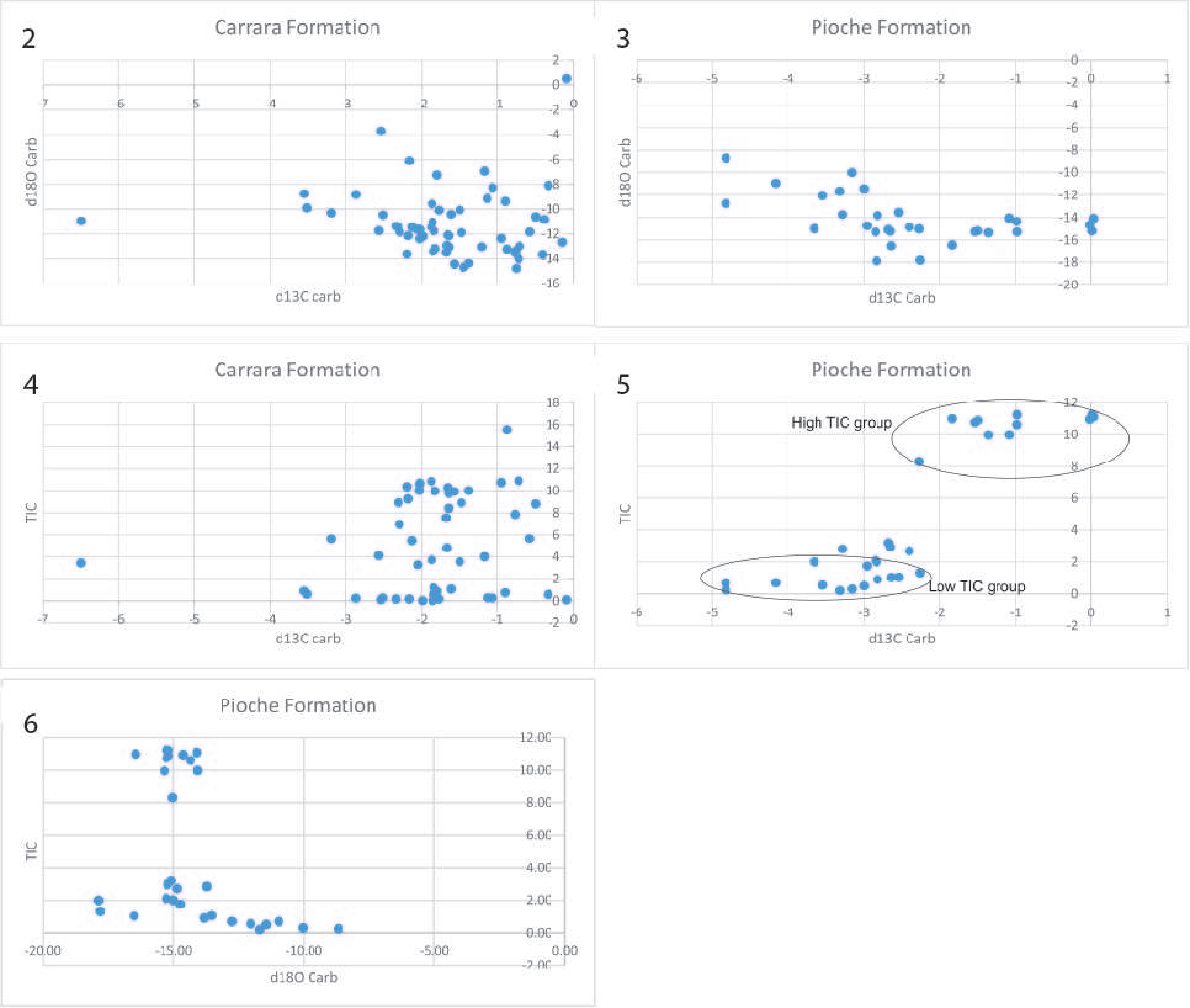
2
Carrara Formation
d18O Carb
d13C carb
3
Pioche Formation
d18O Carb
d13C Carb
4
Carrara Formation
TIC
d13C carb
5
Pioche Formation
High TIC group
Low TIC group
TIC
d13C Carb
6
Pioche Formation
TIC
d18O Carb